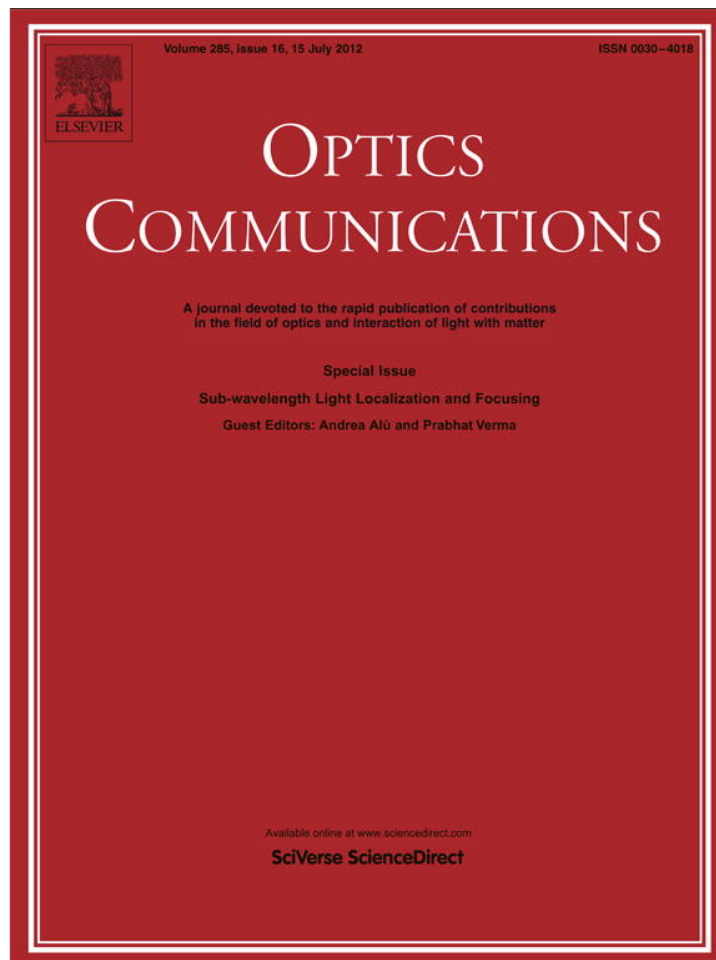


Provided for non-commercial research and education use.
Not for reproduction, distribution or commercial use.



This article appeared in a journal published by Elsevier. The attached copy is furnished to the author for internal non-commercial research and education use, including for instruction at the authors institution and sharing with colleagues.

Other uses, including reproduction and distribution, or selling or licensing copies, or posting to personal, institutional or third party websites are prohibited.

In most cases authors are permitted to post their version of the article (e.g. in Word or Tex form) to their personal website or institutional repository. Authors requiring further information regarding Elsevier's archiving and manuscript policies are encouraged to visit:

<http://www.elsevier.com/copyright>



Diffraction-managed superlensing using plasmonic lattices

Carlos J. Zapata-Rodríguez^{a,*}, David Pastor^a, María T. Caballero^b, Juan J. Miret^b

^a Department of Optics, University of Valencia, Dr. Moliner 50, 46100 Burjassot, Spain

^b Department of Optics, Pharmacology and Anatomy, University of Alicante, P.O. Box 99, Alicante, Spain

ARTICLE INFO

Article history:

Received 3 January 2012

Accepted 7 April 2012

Available online 21 April 2012

Keywords:

Plasmonic devices

Imaging

Superresolution

ABSTRACT

We show that subwavelength diffracted wave fields may be managed inside multilayered plasmonic devices to achieve ultra-resolving lensing. For that purpose we first transform both homogeneous waves and a broad band of evanescent waves into propagating Bloch modes by means of a metal/dielectric (MD) superlattice. Beam spreading is subsequently compensated by means of negative refraction in a plasmon-induced anisotropic medium that is cemented behind. A precise design of the superlens doublet may lead to nearly aberration-free images with subwavelength resolution in spite of using optical paths longer than a wavelength.

© 2012 Elsevier B.V. All rights reserved.

1. Introduction

Plasmonics is gaining current space in groundbreaking photonic technologies since it carries the possibility of molding the flow of subwavelength wave fields. For instance, generation of nanosized hot spots by means of metallic nanoparticles and extraordinary transmission of thin films with subwavelength holes and slits have been extensively analyzed and observed in experiments [1,2]. Relevant applications are high-density waveguiding, nanoantennas, labels for biomedical research and sensing to mention a few [3]. In particular, superlenses are plasmonic flat devices capable of reconstruct a given scattered wave field with subwavelength features [4]. This phenomenon has been applied successfully in high-resolution optical lithography [5,6].

The image formation by metallic single-layer superlenses is based on the excitation of surface plasmons polaritons (SPPs) and anti-plasmons on the entrance and exit interfaces [7]. As a consequence wave amplification inside the metallic slab compensates the attenuation produced in the surrounding dielectric. By coupling a few of these elementary thin lenses we may compose an MD multilayered device capable of transmit high-frequency plane waves by resonant tunneling [8,9]. Assuming a perfect periodic process, a set of evanescent waves is effectively converted into propagating Bloch waves with characteristic pseudo-moment and consequently carrying electromagnetic energy.

Two main concerns are critical in order to achieve a high-fidelity replica of the scattered field. We should prevent first resonant peaks in the transmittance response that would enhance certain spatial frequencies and thus disfiguring the image. Secondly we shall preclude dephasing of different spectral components in the transmission

coefficient. The first issue may be treated essentially by using metals and dielectrics whose permittivities are selectively adjusted, and the second subject is addressed by tuning the filling factors of the materials involved. As a result the wave fields propagate inside the multilayered metallic composites in the canalization regime [10,11].

In this paper we follow a different approach that leads to control dephasing of subwavelength outputs. This is based on counterbalancing the phase response of high-transparent metallic superlenses in order to flatten the overall phase mismatch at the image plane. In geometrical terms, negative refraction of high-frequency Bloch waves excited by a nanosized object contributes to achieve nearly-stigmatic subwavelength imaging. Our study is elicited by a recent direct observation of light focusing through a photonic crystal flat lens designed and fabricated using a III-V semiconductor slab to operate at optical frequencies [12]. More sophisticated devices following the above primitive idea have been presented recently [13]. However the spot size of a reproduced localized field would be diffraction limited clearly. A recent tentative to overcome this limit by using uniform arrays of plasmonic waveguides has been proposed elsewhere [14–16]. Here we do not take into consideration hybrid metal/dielectric media with axial symmetry; on the contrary, we consider multilayered plasmonic devices. We conclude our study by discussing the potential advantages of our proposal.

2. The phase addition rule

In this section we examine the role of elementary flat superlenses in the optical response of two-coupled plasmonic devices. For that purpose let us consider two thin superlenses that for simplicity are immersed in the same transparent medium of dielectric constant ϵ . In principle our approach holds for superlenses that are formed by a single metallic layer, but here we are focused on multilayered structures. When a given P-polarized plane wave of amplitude H_0 and in-plane spatial frequency k_x impinges on the front face of the first

* Corresponding author.

E-mail address: carlos.zapata@uv.es (C.J. Zapata-Rodríguez).

superlens, the wave field is partially transmitted with a complex amplitude $t_1 H_0$. In the case that absorption and reflections are negligible, $|t_1| \approx 1$ for homogeneous waves in the host medium but this is not necessarily true for evanescent fields, where $|k_x| > \sqrt{\epsilon k_0}$ and $k_0 = 2\pi/\lambda_0$ is the wavenumber in vacuum. Propagation along the intermediate medium results in an additional factor $\exp(i\beta L)$, where

$$\beta = \sqrt{\epsilon k_0^2 - k_x^2}, \text{ if } |k_x| \leq \sqrt{\epsilon k_0}, \quad (1)$$

$$\beta = i\sqrt{k_x^2 - \epsilon k_0^2}, \text{ if } |k_x| > \sqrt{\epsilon k_0}. \quad (2)$$

The following step consists of traversing through the second metallic near-field flat lens. Assuming a coefficient of transmission t_2 for the second superlens, the transmitted field yields $H_y = t_1 t_2 \exp(i\beta L) H_0$. More generally, the Airy's formula $H_y = t H_0$, being

$$t = \frac{t_1 t_2 \exp(i\beta L)}{1 - r_1 r_2 \exp(2i\beta L)}, \quad (3)$$

a transmission coefficient, would take into account multiple scattered waves [17], which gives essentially a transmitted field

$$H_y = t_1 t_2 \exp(i\beta L) [1 + r_1 r_2 \exp(2i\beta L) + r_1^2 r_2^2 \exp(4i\beta L) + \dots] H_0, \quad (4)$$

where $r_{1,2}$ is the coefficient of reflection corresponding to a given superlens $SL_{1,2}$. The generalization of the Airy's formula is graphically illustrated in Fig. 1.

In our discussion we shall consider that the flat superlenses SL_1 and SL_2 are firmly attached and, as a consequence, we set $L = 0$ from here on. From Eq. (3) we infer that the phase increment of the transmitted wave H_y with respect to the incident field H_0 is the result of a summation of three terms, corresponding to the arguments of the phasors t_1 , t_2 , and $(1 - r_1 r_2)^{-1}$, respectively. In this paper this is called the phase addition rule. In the case that the modulus of either r_1 or r_2 is significantly lower than unity, the last phasor may be neglected and the phase of the emerging field is directly controlled by the arguments of the transmission coefficients $t_{1,2}$. In this sense, the dependence of $\arg(t_1)$ upon k_x might be compensated with a prescribed superlens SL_2 leading to an ultraflattened curve at least within a given spectral band. Otherwise the argument of $(1 - r_1 r_2)^{-1}$ may transform the overall phase variation in a nonlinear way. Next we consider a procedure to play on the phase addition rule in order to achieve subwavelength aberration-free images.

3. Wave aberration compensation

In Fig. 2 we represent the spectral dependence of the transmission coefficient $t_{1,2}$ both in modulus and phase for a couple of metallodielectric multilayered devices at $\lambda_0 = 485$ nm. Fig. 2(a) shows the transmission

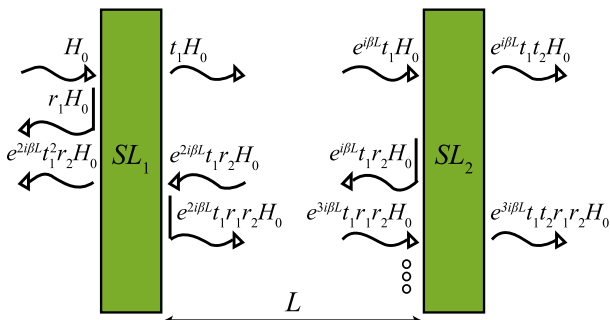


Fig. 1. Illustration of the generalized Airy's formula for two coupled superlenses, SL_1 and SL_2 .

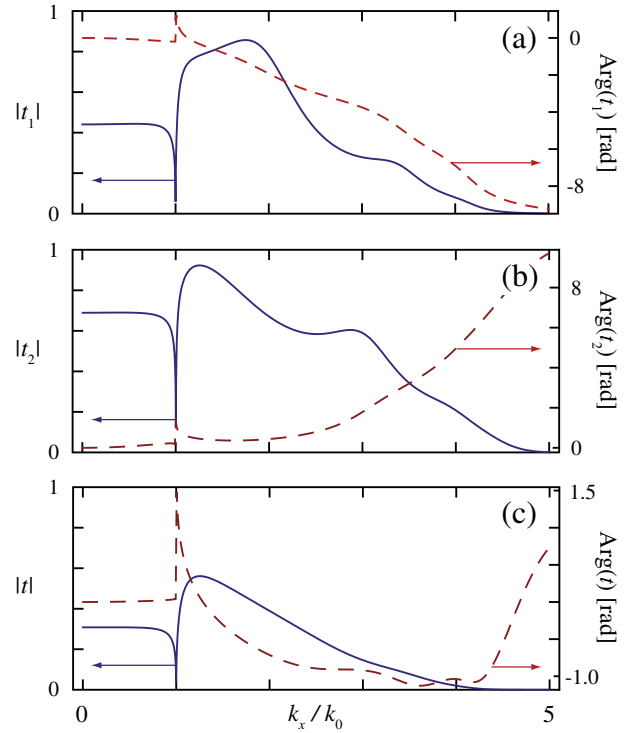


Fig. 2. Transmission coefficient in modulus and phase for finite periodic structures made of silver and a dielectric: (a) SrTiO₃; (b) GaP. In (a) we have $N_1 = 19$ silver layers with a filling factor of $f_1 = 0.35$ within a period of $\Lambda_1 = 30$ nm. In (b) we consider $N_2 = 7$ periods of $\Lambda_2 = 50$ nm for a silver filling factor $f_2 = 0.50$. In both stacked devices the surrounding medium is the vacuum. (c) The transmission coefficient of the coupled structure.

coefficient t_1 for a periodic structure consisting of $N_1 = 19$ silver layers ($\epsilon_{Ag} = -7.754 + i0.727$) hosted in SrTiO₃ ($\epsilon_{SrTiO_3} = 6.596 + i0.070$). A thin metallic slab is symmetrically displaced in the center of the unit cell, which has a period of $\Lambda_1 = 30$ nm, in such a way that the filling factor of silver is $f_1 = 0.35$. Also the surrounding medium of the stack is considered to be the vacuo. Finally, the evaluation of t_1 is carried out by using a standard transfer 2×2 -matrix formalism [17]. From the figure of $|t_1|$ we observe that, in practical terms, our finite lattice cannot transmit spatial frequencies beyond $k_x = \kappa_{SrTiO_3} k_0$, where the effective index of refraction $\kappa_{SrTiO_3} = 4.5$ in our numerical example. Since the refractive index of SrTiO₃, that is $n_{SrTiO_3} = \text{Re}\sqrt{\epsilon_{SrTiO_3}} = 2.57$, is considerably lower than κ_{SrTiO_3} , a resonant tunneling effect driven by SPPs is evident. Moreover, a decreasing variation of the phase of t_1 in terms of k_x is clearly revealed. In Fig. 2(b) we depict the transmission coefficient t_2 for a second lattice made of $N_2 = 7$ silver slabs placed on GaP ($\epsilon_{GaP} = 13.287$). In this case the period is $\Lambda_2 = 50$ nm and the filling factor of silver is $f_2 = 0.50$. While the effective index of refraction κ_{GaP} is comparable with that obtained in the previous case, the phase shows a completely different behavior. Now the complex argument of the transmittance increases for higher spatial frequencies k_x . Note also that the phase increment observed in the GaP lattice goes around 3π rads, which approximately corresponds to the phase decrement attributed to the SrTiO₃ multilayer. Then a compensated-phase response. This finding is confirmed in Fig. 2(c) where the net phase deviation of the transmission coefficient t is always lower than π rads within the effective bandwidth $|k_x| < \kappa k_0$, where $\kappa = 4.5$ once again.

The different behavior observed in the phase dependence of transmittances $t_{1,2}$ upon transverse spatial frequencies k_x may be explained from the isofrequency curves of the periodic lattices. In Fig. 3 we represent the dispersion equation [17]

$$\cos(k_z \Lambda) = \cos\varphi_1 \cos\varphi_2 - \eta \sin\varphi_1 \sin\varphi_2, \quad (5)$$

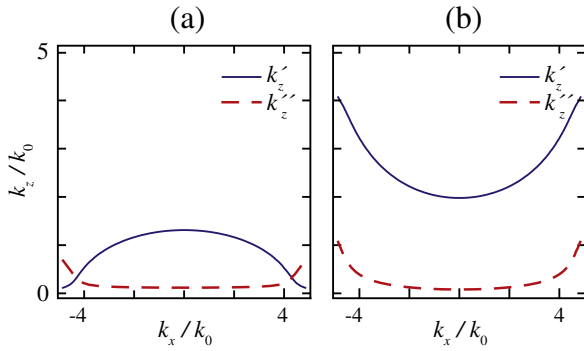


Fig. 3. Isofrequency curves given from Eq. (5) for the hybrid silver-dielectric periodic media containing (a) SrTiO₃ and (b) GaP. Note that k'_z and k''_z are the real part and the imaginary part of k_z , respectively.

corresponding to P-polarized waves propagating within an infinite periodic multilayered structure, where the metal-dielectric interfaces are parallel to the xy plane. Furthermore the component $k_z = k'_z + ik''_z$ of the wave vector represents a Bloch pseudo-moment. In Eq. (5) the period $\Lambda = d_1 + d_2$ stands for the width of the silver slab plus that corresponding to the dielectric medium under consideration, $\varphi_q = k_{qz}d_q$ with $q = \{1, 2\}$ representing either the dielectric or the metal,

$$\eta = \frac{1}{2} \left(\frac{\epsilon_1 k_{2z} + \epsilon_2 k_{1z}}{\epsilon_2 k_{1z} + \epsilon_1 k_{2z}} \right), \quad (6)$$

and finally assuming $k_y = 0$, then

$$k_{qz}^2 + k_x^2 = \epsilon_q k_0^2 \quad (7)$$

represents the dispersion equation within each bulk medium. From Fig. 3 we infer that the superlattice made of SrTiO₃ has an isofrequency curve with normal negative curvature. The propagator $\exp(ik'_z z)$ indicates that the dephase accumulated by a wave field is directly proportional to k'_z . Neglecting impedance mismatch at the input and output planes of the multilayered device, we expect that the dependence of k'_z upon k_x follows the same variation observed in the argument of the transmission coefficient t_1 upon k_x . Figs. 2(a) and 3(a) indicate that this is in good agreement up to the normalized cutoff frequency κ given by the solution of the equation $k'_z(\kappa k_0) = k''_z(\kappa k_0)$ that is $\kappa = 4.3$. Note that κ represents essentially the effective index of refraction κ_{SrTiO_3} described above. Next we may follow a similar procedure to relate the isofrequency curve given in Fig. 3(b), which corresponds to the periodic medium containing GaP, with the phase spectral dependence of the transmission coefficient t_2 given in Fig. 2(b). In this case we conclude that the positive curvature of the dispersion equation explains the phase increment observed at higher spatial frequencies k_x .

Phase compensation attributed to coupling of two MD superlattices with isofrequencies of opposite curvature also renders a geometrical interpretation of our results. For the sake of clarity let us consider the propagation direction of a monochromatic wave packet with carrier spatial frequency k_{x0} . This wave field flies within a periodic medium along a direction given by the normal vector $\vec{N} = (N_x, N_z)$, which is calculated from the isofrequency curve in terms of the group velocity $\vec{v}_g = \nabla k\omega$ in the vicinities of k_{x0} and $\omega_0 = k_0 c$, being c the speed of light in vacuum. Assuming that the field propagates in the positive direction of the z axis, that is $N_z > 0$, we find that the sign of N_x exclusively depends on the sign of the isofrequency curvature. As a consequence, the wave packet that pass through the interface joining both MD superlattices experiences negative refraction. This is illustrated in Fig. 4 for a wave packet of carrier frequency (a) $k_{x0} = k_0$ and (b) $k_{x0} = 3k_0$. Our numerical simulations are performed with a commercial software based on finite-element methods (FEMs). Since attenuation driven by losses in silver makes difficult a clear observation of the wave-packet trajectory, also

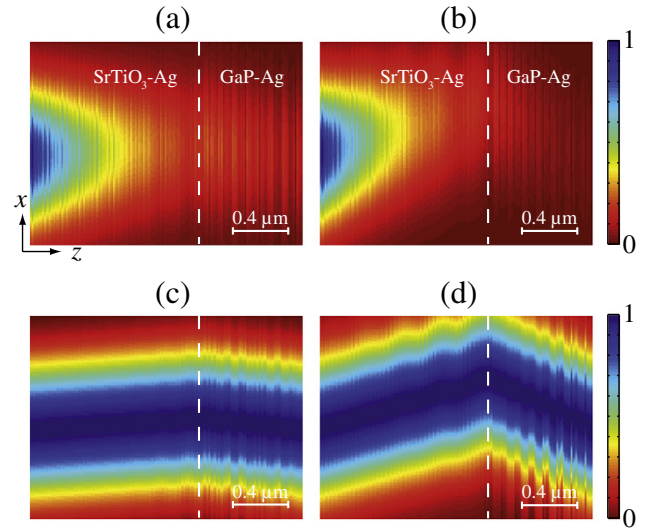


Fig. 4. FEM simulations shown negative refraction on the surface (black dashed line) that joins the MD superlattice including SrTiO₃, set on the left, and that containing GaP. Sub-figures (c) and (d) result from normalizing the modulus of the magnetic field $|H_y|$ plane by plane.

we depict the transverse magnetic field normalized in such a way that the maximum value of $|H_y|$ at a given plane $z = z_0$ is always the unity.

When the fields propagate within the lattice composed of SrTiO₃, the angles corresponding with each vector \vec{N} as measured with respect to the z axis are numerically estimated from Fig. 3(a) and (b) giving $\theta_1 = +0.07$ rad and $\theta_1 = +0.28$ rad, respectively. Note that these angles are significantly small. If the wave packets travel through the multilayered medium containing GaP, now these angles yield $\theta_2 = -0.12$ rad and $\theta_2 = -0.44$ rad, respectively. Let us point out that the parameter

$$C = \frac{\tan\theta_1}{\tan\theta_2} \quad (8)$$

takes a value approaching -0.62 in both cases. Moreover C is a quantity that is approximately conserved for $|k_x| < 3.5k_0$, as shown in Fig. 5. This result provides a significant contribution to our geometrical interpretation of the proposed diffraction-managed imaging. A light ray emerging from a point on axis that propagates from a plane $z = 0$ to $z = L_1$ in the first medium and, immediately after, travels in the second medium up to $z = L_1 + L_2$, such that $C = -L_2/L_1$ holds, gets its way back to the z axis. Note that $L_{1,2} = N_{1,2} \Lambda_{1,2}$ in our numerical case, and that we have $-L_2/L_1 = -0.614$.

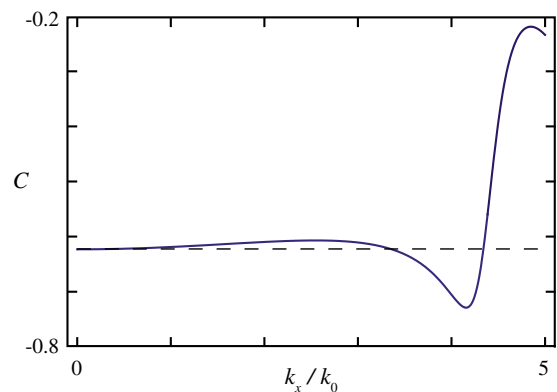


Fig. 5. Dependence of the parameter C , defined in Eq. (8), on the spatial frequency k_x . Note that C is practically invariant within the spectral domain $|k_x| < 3.5k_0$.

As mentioned above, invariance of C holds for a wide spectral range. This is important if we consider a localized source in the input interface of the first MD finite lattice. The light rays emerging from this point object are conveniently deviated, by means of negative refraction, at the surface that joins the periodic media involved. As a consequence all these rays are focused precisely at the exit plane $z=L_1+L_2$. In other words, the condition of stigmatism is approximately satisfied so that nearly aberration-free images may be formed by our device. We point out that spherical aberration is not completely removed in this study, which is clearly seen in the spectral band $3.5 < |k_x| < 4.5$. As a result it shall finely decrease the resolving power of the imaging system [18].

This is illustrated in Fig. 6 by using FEM simulations in COMSOL Multiphysics 3.5. In front of our device we insert a Cr layer whose width is 100 nm. Also the Cr film has a centered slit aperture whose width takes a value of 20 nm in Fig. 6(a). A P-polarized plane wave collides with the Cr film that collects part of the light, which subsequently is guided toward the entrance surface of the diffraction-managed superlens. Thus the deep-subwavelength wave field in the input is diffracted inside the first multilayered medium; immediately after reaching the GaP superlattice it is continuously compressed along the transverse direction. The output magnetic field consists of a strong central lobe whose FWHM is $\rho=130$ nm, that represents only $0.27 \lambda_0$. This confirms the subwavelength character of the image-formation process in spite of the fact that the object plane and the image plane are separated by a distance of 950 nm that supposes barely twice the wavelength λ_0 . We have repeated the FEM simulations for other slit widths, and we have observed that the response of the superlensing device is practically the same whether the slit width is substantially smaller than ρ . Therefore ρ stands for the limit of resolution of the superlensing coupled device. For wider slits, on the contrary, the magnetic field at the output plane resembles that at the input plane. In Fig. 6(b) we show the wave field for a slit aperture of 200 nm. In this case, the beam width that is excited by the plasmonic slit is conserved not only at the exit but also all along the periodic media. This canalization regime is the result of the strong anisotropy of the two superlattices involved, as shown in Fig. 3. Thus, the low frequency of the spatial spectrum associated with the scattered electromagnetic waves at the input plane leads to the dominant self-collimation of the electromagnetic flow.

To estimate the limit of resolution we alternatively employ the impulse response also known as point spread function (PSF) [19]. The 1D PSF is simply the Fourier transform of the amplitude transfer

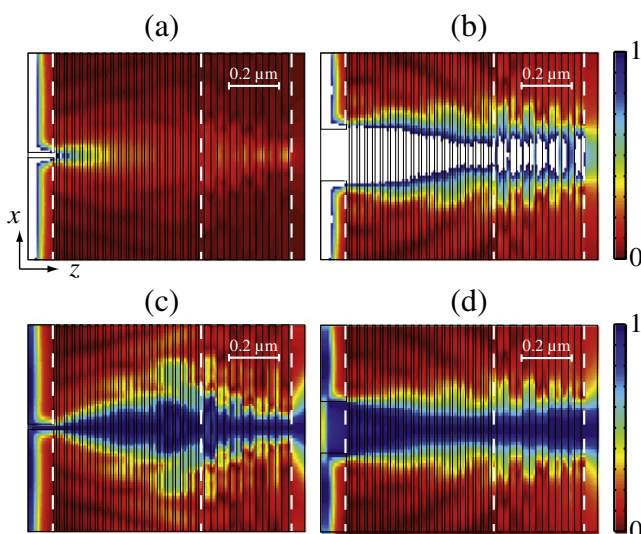


Fig. 6. FEM simulations shown superlensing of the device composing the MD superlattice including SrTiO_3 , set on the left, and that containing GaP. In (a) the slit width is 20 nm and in (b) the slit width is 200 nm. For the sake of clarity, again we show the modulus of the magnetic field in (c) and (d) as it is normalized plane by plane.

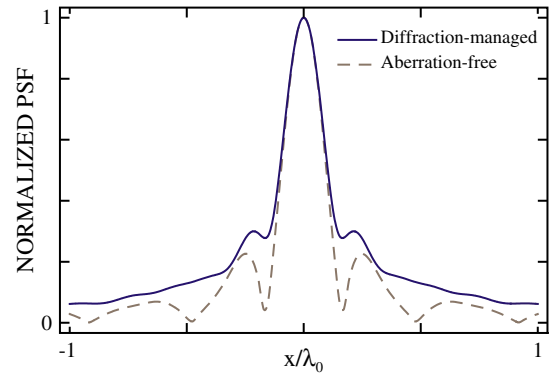


Fig. 7. Modulus of the 1D PSF at the image plane of our diffraction-managed superlens. The 1D PSF of an aberration-free system maintaining the same $|t|$ is also represented graphically.

function, that for two coupled stratified devices it is simply the transmission coefficient $t(k_x)$ given in Eq. (3). The PSF averages the response of harmonic signals provided an equienergetic set of P-polarized plane waves of different transverse spatial frequencies k_x impinges onto the plasmonic multilayers. Strictly speaking the 1D PSF is valid for line sources instead of point sources, the latter case treated elsewhere [20,21]. In mathematical terms we write [22]

$$h(x) = \frac{1}{2\pi} \int_{-\infty}^{\infty} t(k_x) \exp(ik_x x) dk_x. \quad (9)$$

Fig. 7 depicts $|h(x)|$ that represents the modulus of the 1D PSF at the image plane of our diffraction-managed device. The FWHM of the central peak yields $0.214 \lambda_0$, which is very close to limit of resolution ρ obtained from FEM-based numerical simulations. For the sake of completeness we also have represented the 1D PSF for a purely aberration-free setup with the same transmission strength $|t|$ as shown in Fig. 2(c). Therefore the argument of the transmission coefficient is set arbitrarily constant. After performing the corresponding 1D Fourier transform of $|t(k_x)|$ we estimate that the FWHM of the diffraction-free 1D PSF decreases up to a value of $0.195 \lambda_0$. We conclude that the 1D impulse response is not broadened significantly due to residual phase offset. In general terms we find that the 1D PSF is weakly blurred, which is confirmed by simply inspection of the small strength associated with its closest sidelobes. This fact is of relevance in coherent imaging of either localized scatterers or extended objects.

4. Conclusions

We conclude that management of subwavelength diffracted wave fields may be employed in multilayered metallic lenses to obtain superresolution. A first MD superlattice with strong anisotropy converts evanescent fields into propagating Bloch modes. Beam spreading is compensated by means of negative refraction. For that purpose, a second MD superlattice with an isofrequency curve of opposite curvature collects the wide spectrum of some Bloch waves and, subsequently, they are suitably focused just at the output plane of the superlensing device. Although our results are highly satisfactory, the simplicity of our proposal paves the way for further improvements up to a certain degree, which shall be considered in future studies.

Acknowledgments

This research was funded by the Spanish Ministry of Science and Innovation (MCIIN) under the project TEC2009-11635.

References

- [1] T. Klar, M. Perner, S. Grosse, G. von Plessen, W. Spirkl, J. Feldmann, *Physical Review Letters* 80 (1998) 4249.
- [2] L. Martín-Moreno, F.J. García-Vidal, H.J. Lezec, K.M. Pellerin, T. Thio, J.B. Pendry, T. Ebbesen, *Physical Review Letters* 86 (2001) 1114.
- [3] M.I. Stockman, *Optics Express* 19 (2011) 22029.
- [4] J.B. Pendry, *Physical Review Letters* 85 (2000) 3966.
- [5] N. Fang, H.S. Lee, C. Sun, X. Zhang, *Science* 308 (2005) 534.
- [6] D.O.S. Melville, R.J. Blaikie, *Optics Express* 13 (2005) 2127.
- [7] J.B. Pendry, S.A. Ramakrishna, *Physica B: Condensed Matter* 338 (2003) 329.
- [8] M. Scalora, M.J. Bloemer, A.S. Pethel, J.P. Dowling, C.M. Bowden, A.S. Manka, *Journal of Applied Physics* 83 (1998) 2377.
- [9] E. Shamonina, V.A. Kalinin, K.H. Ringhofer, L. Solymar, *Electronics Letters* 37 (2001) 1243.
- [10] P.A. Belov, Y. Hao, *Physical Review B: Condensed Matter* 73 (2006) 113110.
- [11] A. Pastuszczak, R. Kotyński, *Journal of Applied Physics* 109 (2011) 084302.
- [12] N. Fabre, L. Lalouat, B. Cluzel, X. Mélique, D. Lippens, F. de Fornel, O. Vanbésien, *Physical Review Letters* 101 (2008) 073901.
- [13] S. Kocaman, M.S. Aras, P. Hsieh, J.F. McMillan, C.G. Biris, N.C. Panoiu, M.B. Yu, L. Kwong, A. Stein, C.W. Wong, *Nature Photonics* 5 (2011) 499.
- [14] M. Conforti, M. Guasoni, C.D. Angelis, *Optics Letters* 33 (2008) 2662.
- [15] Y. Liu, G. Bartal, X. Zhang, *Optics Express* 16 (2008) 15439.
- [16] C. Yan, D.H. Zhang, Y. Zhang, D. Li, M.A. Fiddy, *Optics Express* 18 (2010) 14794.
- [17] P. Yeh, *Optical Waves in Layered Media*, Wiley, New York, 1988.
- [18] C.J. Zapata-Rodríguez, D. Pastor, J.J. Miret, in: V. Kuzmiak, P. Markos, T. Szoplík (Eds.), *Proc. SPIE*, vol. 8070, 2011, p. 807041.
- [19] J.W. Goodman, *Introduction to Fourier Optics*, 2nd ed. McGraw-Hill International Editions, Singapore, 1996.
- [20] C.J. Zapata-Rodríguez, D. Pastor, J.J. Miret, *Applied Optics* 49 (2010) 5870.
- [21] C.J. Zapata-Rodríguez, D. Pastor, V. Camps, M.T. Caballero, J.J. Miret, *Journal of Nanophotonics* 5 (2011) 051807.
- [22] R. Kotyński, *Opto-Electronics Review* 18 (2010) 366.